

# The Effect of Nuclear-Quadrupole Coupling in the Laser-Induced Alignment of Molecules

Linda V. Thesing,<sup>1,2,3</sup> Andrey Yachmenev,<sup>1,2, a)</sup> Rosario González-Férez,<sup>4, b)</sup> and Jochen Küpper<sup>1,2,3, c)</sup>

<sup>1)</sup>Center for Free-Electron Laser Science, Deutsches Elektronen-Synchrotron DESY, Notkestrasse 85, 22607 Hamburg, Germany

<sup>2)</sup>The Hamburg Center for Ultrafast Imaging, Universität Hamburg, Luruper Chaussee 149, 22761 Hamburg, Germany

<sup>3)</sup>Department of Physics, Universität Hamburg, Luruper Chaussee 149, 22761 Hamburg, Germany

<sup>4)</sup>Instituto Carlos I de Física Teórica y Computacional and Departamento de Física Atómica, Molecular y Nuclear, Universidad de Granada, 18071 Granada, Spain

(Dated: 16 October 2021)

**Abstract:** We present a theoretical study of the time-dependent laser alignment of molecules taking into account the hyperfine coupling due to nuclear-quadrupole interactions. The coupling of nuclear spins to the overall angular momentum of molecules significantly influences their rotational dynamics. Here, we systematically analyze the impact of the nuclear-quadrupole coupling on the rotational dynamics of the linear  $I_2$  and the asymmetric-top diiodobenzene molecule induced by external laser fields. We explore different regimes of pulse shapes and laser-pulse intensities and detail under which conditions the quadrupole coupling cannot be neglected in the description of the laser alignment of molecules.

## I. Introduction

Controlling the rotational motion of molecules with external electric fields is among the most interesting goals in physical chemistry. The simplest approach to theoretically describe this field-induced control relies on applying the rigid-rotor approximation. For many molecular species, this approach has been shown to be sufficient,<sup>1–5</sup> even for some floppy molecules.<sup>6</sup> However, the coupling of the overall angular momentum to additional angular momenta or internal rotations cannot be neglected under certain circumstances. For instance, it has been shown that coupling of nuclear spins and the overall angular momentum can have a significant impact on the rotational dynamics on experimentally relevant timescales.<sup>7–15</sup>

Fixing molecules in space, i. e., aligning and orienting them,<sup>16–18</sup> is of particular interest among rotational control schemes as it reduces the blurring of experimental observables caused by averaging over the random orientations and allows to obtain information in the molecular frame.<sup>19–21</sup> Molecules can be aligned by subjecting them to nonresonant laser fields. If the laser pulse is switched on slowly compared to the molecular rotational period, adiabatic alignment is achieved. On the other hand, by using short laser pulses, coherent superpositions of field-free rotational states are created. The wave packets rephase periodically and show revivals of the alignment in field-free space.<sup>1,22–24</sup> Such coherent superpositions can also be obtained by shaped laser pulses which are turned off rapidly compared to the rotational period of the molecule.<sup>25–29</sup>

Recently, it has been shown that the impulsive alignment of  $I_2$  molecules can only be described accurately if

the nuclear-quadrupole coupling is taken into account.<sup>30</sup> We previously developed a generalized methodology to describe the rovibrational dynamics of molecules including nuclear-quadrupole interactions.<sup>31</sup> Here, we systematically analyze the impact of this coupling in different existing techniques for laser alignment of prototypical linear and asymmetric top molecules using  $I_2$  and 1,4-diiodobenzene as examples. Our results thereby serve as a guideline to understand under which circumstances the quadrupole coupling has a significant influence on the rotational dynamics.

## II. Theoretical Description

In  $I_2$  and 1,4-diiodobenzene (DIB), the interaction between the nuclear quadrupole moments of two equivalent iodine  $^{127}I$  nuclei and the electric field gradients, arising from the charge distributions of the surrounding nuclei and electrons, lead to the well known hyperfine splittings of the rotational energy levels. Each rotational level of the molecule is thus split into a maximum of 36 sub-levels, labeled by the quantum number  $F$  of the total angular momentum operator  $\mathbf{F} = \mathbf{J} + \mathbf{I}$ , where  $\mathbf{J}$  is the rotational angular momentum neglecting the spin, which for the molecules considered here is the angular momentum of overall rotation. Here,  $\mathbf{I} = \mathbf{I}_1 + \mathbf{I}_2$  is the collective nuclear spin angular momentum operator with  $I_1 = I_2 = 5/2$  and thus  $0 \leq I \leq 5$ .

The theoretical model for the nuclear-quadrupole interactions has been described before.<sup>31</sup> Briefly, within the Born-Oppenheimer and semirigid-rotor approximations, the field-free Hamiltonian can be written as

$$H_{\text{mol}} = H_{\text{rot}} + \sum_{l=1,2} \mathbf{V}(l) \cdot \mathbf{Q}(l), \quad (1)$$

where  $H_{\text{rot}}$  is the semirigid-rotor Hamiltonian. The rotational constant of  $I_2$  was experimentally determined to

<sup>a)</sup>andrey.yachmenev@cfel.de

<sup>b)</sup>rogonzal@ugr.es

<sup>c)</sup>Email: jochen.kuepper@cfel.de;

website: <https://www.controlled-molecule-imaging.org>

$B = 1118.63$  MHz.<sup>30</sup> For DIB, the rotational constants  $B_z = A = 5712.768$  MHz,  $B_y = B = 159.017$  MHz, and  $B_x = C = 154.710$  MHz were obtained from a geometry optimization using density functional theory (DFT) with the B3LYP functional and the def2-QZVPP basis set;<sup>32,33</sup> for the iodine atoms the effective core potential def2-ECP was used.<sup>34</sup> All electronic structure calculations employed the quantum-chemistry package ORCA.<sup>35,36</sup> The molecule-fixed frame (MFF),  $x, y, z$ , is defined by the principal axes of inertia. In the second term,  $\mathbf{Q}(l)$  is the nuclear-quadrupole tensor of the  $l$ -th iodine nucleus and  $\mathbf{V}(l)$  is the electric-field-gradient tensor at the instantaneous position of the corresponding nucleus. Due to the symmetry of DIB, the electric-field-gradient (EFG) tensors on the two iodine centers are equal to each other with nonzero elements only on the diagonal  $V_{xx} = -5.5879$  a. u.,  $V_{yy} = -6.2295$  a. u. and  $V_{zz} = 11.8174$  a. u.. The nuclear quadrupole moment for  $^{127}\text{I}$  is  $Q = -696$  mb.<sup>37</sup> For  $\text{I}_2$ , instead of computing the EFG tensors we used the experimental nuclear-quadrupole coupling constant  $\chi_{zz} = eQV_{zz} = -2.45258$  GHz,<sup>38</sup> with the elementary charge  $e$ .

The interaction of a molecule with a nonresonant laser field, linearly polarized along the laboratory-fixed  $Z$  axis, is given by

$$H_{\text{las}}(t) = -\frac{I(t)}{2\epsilon_0 c} \alpha_{ZZ} \quad (2)$$

where  $\alpha_{ZZ}$  is the element of the polarizability tensor of the molecule along the laser polarization axis. The polarizabilities defined in the laboratory frame are directly transformed to the molecular frame  $\alpha_{ij}$  ( $i, j = x, y, z$ ).<sup>39</sup> For both,  $\text{I}_2$  and DIB, the polarizability tensor  $\alpha_{ij}$  is diagonal in the inertial frame. For  $\text{I}_2$ , we used the values  $\alpha_{xx} = \alpha_{yy} = 7.94 \text{ \AA}^3$  and  $\alpha_{zz} = 13.96 \text{ \AA}^3$ .<sup>40</sup> For DIB, calculated values of  $\alpha_{xx} = 11.307 \text{ \AA}^3$ ,  $\alpha_{yy} = 16.676 \text{ \AA}^3$ , and  $\alpha_{zz} = 32.667 \text{ \AA}^3$  were used<sup>41</sup>. Calculations of the EFG and polarizability tensors for the DIB molecule were carried out at the DFT/B3LYP level of theory using the all-electron scalar relativistic Douglas-Kroll-Hess Hamiltonian<sup>42</sup> with the DKH-def2-TZVP basis set.<sup>43,44</sup>

To study the rotational dynamics of  $\text{I}_2$  and DIB, we solved the time-dependent Schrödinger equation (TDSE) for the full Hamiltonian

$$H(t) = H_{\text{mol}} + H_{\text{las}}(t). \quad (3)$$

The time-dependent wave function was built from a superposition of the field-free spin-rotational eigenfunctions of  $H_{\text{mol}}$ . The time-dependent coefficients were determined by numerical solution of the TDSE using the split-operator method using RichMol.<sup>39</sup> To obtain the field-free eigenfunctions, we solved the time-independent Schrödinger equation for the Hamiltonian  $H_{\text{mol}}$ . The matrix representation of  $H_{\text{mol}}$  was constructed in a symmetry-adapted coupled basis  $|F, J, I, w\rangle$  of the rotational wave functions  $|J, w\rangle$  and the nuclear-spin functions  $|I\rangle$ . Here,  $w$  represents additional rotational (pseudo) quantum numbers,

such as  $K_a$  and  $K_c$  for DIB. For  $\text{I}_2$ , we took into account the symmetry requirement that  $J$  and  $I$  have to be either both even or both odd,<sup>45</sup> while for DIB all combinations of basis states are allowed. The rotational states  $|J, w\rangle$  were obtained as linear combinations of symmetric top functions by diagonalizing  $H_{\text{rot}}$ . The explicit expressions for the matrix elements of the quadrupole coupling Hamiltonian and various multipole Cartesian tensor operators can be found elsewhere.<sup>31,46,47</sup> To obtain the matrix representation of the interaction Hamiltonian, the matrix elements were first set up in the coupled basis<sup>46</sup> and then transformed to the field-free eigenbasis.<sup>31</sup> The alignment is quantified by  $\langle \cos^2\theta \rangle$ , with the Euler angle  $\theta$  between the molecule-fixed  $z$  and the laboratory-fixed  $Z$  axes.

### III. Results and Discussion

**Adiabatic alignment** We considered a linearly polarized laser pulse with a Gaussian envelope  $I(t) = I_0 \exp(-4 \ln 2 t^2 / \tau_{\text{FWHM}}^2)$ , where  $\tau_{\text{FWHM}} = 8$  ns and  $I_0 = 2 \times 10^{11}$  W/cm<sup>2</sup>. For the rotational temperature  $T_{\text{rot}} = 0$  K, we assumed that all hyperfine states corresponding to the rotational ground state  $J = 0$  were populated according to their statistical weights. For  $\text{I}_2$ , the spin-rotational states with even  $I$  have equal weights while the ones with odd  $I$  have zero weights.<sup>45</sup> For DIB, the Hydrogen nuclear-spin functions result in weights of 7 (3) for even (odd)  $I$ ; see Appendix A. The adiabatic alignment with nuclear-quadrupole coupling was computed by averaging over individually obtained alignment results for the 15 (36) initial nuclear-spin states of  $\text{I}_2$  (DIB).

The interaction of the external electric field with the polarizability of the molecules is much stronger than the quadrupole-coupling interaction, resulting in the decoupling of the nuclear spins from the overall-rotation angular momentum. As a result, the influence of the nuclear-quadrupole coupling on the adiabatic alignment is negligible for both molecules. At the peak intensity, we thus obtained  $\langle \cos^2\theta \rangle = 0.946$  and  $\langle \cos^2\theta \rangle = 0.988$  for  $\text{I}_2$  and DIB, respectively, both, including and neglecting the quadrupole coupling.

**Impulsive alignment** We analyzed the impulsive alignment induced by short ( $\tau_{\text{FWHM}} = 1$  ps) nonresonant linearly polarized laser pulses with Gaussian envelopes. We compared the post-pulse dynamics including and neglecting the nuclear-quadrupole coupling for the rotational ground states, i. e.,  $T_{\text{rot}} = 0$  K. To allow for a better comparison of the alignment with and without the coupling, we used initial states with well defined rotational quantum numbers, i. e., uncoupled states  $|IM_I\rangle |00\rangle$  ( $|IM_I\rangle |0_{00}0\rangle$ ) for  $\text{I}_2$  (DIB), and averaged over the results for the different spin isomers, see above. We point out that the corresponding field-free eigenstates have contributions of  $J > 0$  rotational states, which might lead to additional differences in the dynamics. To solve the TDSE, we

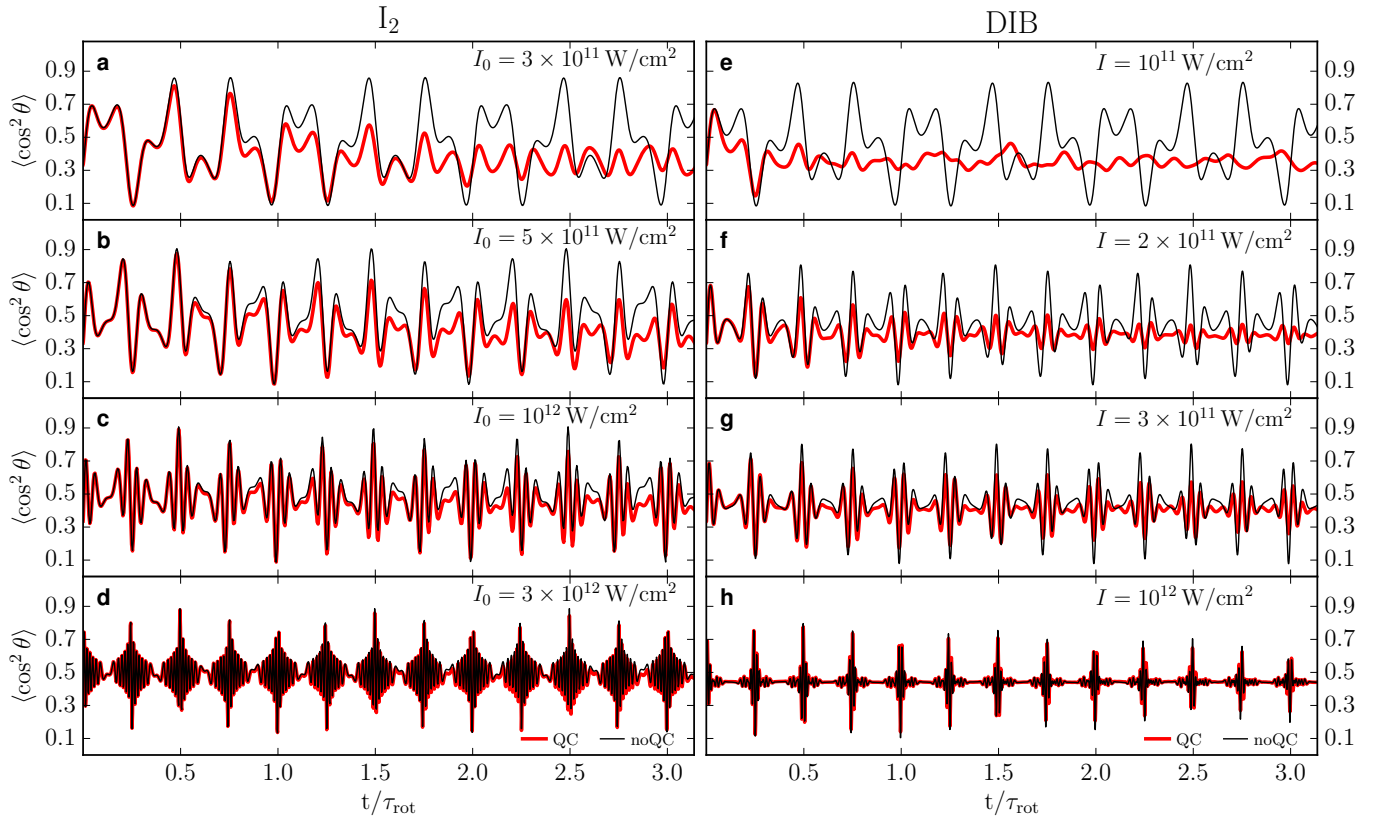


FIG. 1. Impulsive alignment induced by laser pulses with  $\tau_{\text{FWHM}} = 1$  ps for (a–d)  $\text{I}_2$  and (e–h) DIB including (QC) and neglecting the nuclear-quadrupole coupling (noQC). The expectation value  $\langle \cos^2 \theta \rangle$  is shown as a function of  $t/\tau_{\text{rot}}$ , where  $\tau_{\text{rot}}$  is the rotation period of the molecules. For each row, the laser intensities were chosen to create rotational wave packets involving similar distributions of  $J$  values for both molecules when the quadrupole coupling is neglected.

projected each initial state onto the field-free eigenbasis.

Fig. 1 shows the post-pulse alignment for (a–d)  $\text{I}_2$  for intensities  $3 \times 10^{11} \text{ W/cm}^2 < I_0 < 3 \times 10^{12} \text{ W/cm}^2$  and (e–h) DIB for intensities  $10^{11} \text{ W/cm}^2 < I_0 < 10^{12} \text{ W/cm}^2$  as a function of time in units of the rotational periods,  $\tau_{\text{rot}} = 446.98$  ps and  $\tau_{\text{rot}} = 3187.48$  ps for  $\text{I}_2$  and DIB, respectively. The post-pulse alignment simulated without the quadrupole interaction shows typical revival structures for rotational wave packets induced by short laser pulses. For the smallest intensities, Fig. 1 a, e, the field-dressed dynamics is dominated by a few low-energy rotational states and  $\langle \cos^2 \theta \rangle$  oscillates with the period  $\tau_{\text{rot}}$ . For DIB and  $I_0 = 10^{11} \text{ W/cm}^2$ , contributions of rotational states with  $K_a > 0$  are negligible and the post-pulse dynamics is similar to the one of the linear molecule  $\text{I}_2$ . With increasing intensity  $I_0$ , more highly excited rotational states are involved in the dynamics. The rotational dynamics of DIB in Fig. 1 h shows a decrease of the peak alignment over time resulting from the asymmetry splitting of rotational states with  $K_a > 0$ .<sup>2,48</sup>

The effect of the nuclear-quadrupole coupling on the alignment depends strongly on the laser intensity. For the low intensities in Fig. 1 a, e it is strongest and the field-free alignment decreases over time for both  $\text{I}_2$  and DIB. However, during the short pulse the quadrupole in-

teraction plays a negligible role for both molecules due to a decoupling of the nuclear spin and overall-rotation angular momenta. The laser field only affects the rotational part of the wave packet, leaving the nuclear-spin quanta unchanged. As a consequence, the alignment traces with and without the quadrupole coupling are very similar to each other directly after the laser pulse. This also holds for higher laser intensities.

For DIB, the alignment then decreases quickly after the pulse, while for  $\text{I}_2$  the rotational dynamics starts to differ at  $t \approx \tau_{\text{rot}}/2$ . This decrease in the field-free alignment for small intensities can be rationalized in terms of the hyperfine energy levels of the Hamiltonian (1). For the low-energy rotational states, which contribute most to the dynamics in Fig. 1 a, e, the hyperfine-splitting patterns depend strongly on  $J$ . These irregular patterns introduce incommensurate frequencies that lead to a dephasing of the wave packet, thus preventing strong revivals of the alignment. In contrast to  $\text{I}_2$ , for DIB the energy differences of hyperfine components within the low-energy rotational states are similar to the energy differences between the rotational levels themselves and strong inter- $J$  coupling is observed in the spin-rotational states. As a consequence, the alignment of DIB is affected much more strongly and faster, with respect to the rotational timescale, than it is

for  $I_2$ .

The influence of the quadrupole coupling can also be interpreted using a classical picture. The precession of  $\mathbf{I}$  and  $\mathbf{J}$  around  $\mathbf{F}$  results in a variation of their projections  $M_J$  and  $M_I$ , leading to a decrease of the alignment. In addition, the magnitudes  $|\mathbf{I}|$  and  $|\mathbf{J}|$  are changed over time by the quadrupole coupling, further affecting the rotational dynamics. Note that for  $I_2$ , the changes in  $|\mathbf{J}|$  are very small but a change in  $|\mathbf{I}|$  still affects the spatial orientation of  $\mathbf{J}$ , since the total angular momentum  $\mathbf{F}$  is preserved.

As the laser intensity was risen, Fig. 1 b–d, f–h, the influence of the quadrupole interaction diminished for both molecules. In Fig. 1 d, h, minor differences can only be observed after the first rotational period. For these strong fields, highly excited states with up to  $J \approx 44$  (and  $K_a \approx 10$  for DIB) dominate the post-pulse dynamics, for which the hyperfine patterns become increasingly uniform.<sup>49,50</sup> For these large  $J$ , the matrix elements of  $\cos^2\theta$  that contribute significantly to the alignment are those between field-free eigenstates with  $\Delta F = \Delta J$  and the same nuclear-spin contributions. Since the hyperfine energy shifts are approximately the same for these states, their energy gaps are very similar to those between the corresponding rotational levels. As a result, we observe only a very weak dephasing in Fig. 1 d, h.

If field-free eigenstates are used as initial states, the averaged alignment results for  $I_2$  do not differ significantly from the result in Fig. 1. For DIB on the other hand, we observe small deviations originating from a considerable mixing of different  $J$ -states in the hyperfine eigenstates, modifying the initial rotational wave function. The impact of the quadrupole interaction is, however, qualitatively the same. The different sets of initial states can only be considered equivalent when the result is averaged over all different spin isomers and  $M$ -states for a given rotational level. Individual eigenstates are in general linear combinations of uncoupled states with different values of  $I$ ,  $M_I$  and  $M_J$ , even if the coupling of different  $J$ -states by the quadrupole interactions is neglected.

**Truncated pulse alignment** For asymmetric top molecules, truncated laser pulses typically allow one to obtain larger degrees of field-free alignment than short laser pulses, taking advantage of the initial adiabatic alignment.<sup>25,29</sup> Here, we consider a laser pulse with a rising and falling edge, both with a Gaussian shape corresponding to  $\tau_{\text{FWHM}} = 600$  ps and  $\tau_{\text{FWHM}} = 2$  ps, respectively, and a peak intensity of  $I_0 = 5 \times 10^{11} \text{ W/cm}^2$ .

The alignment results for  $I_2$  and DIB as a function of  $t/\tau_{\text{rot}}$  are shown in Fig. 2 a, b, respectively. For both molecules, strong alignment was reached before the cut-off of the laser field with  $\langle \cos^2\theta \rangle$  close to 1. As in the adiabatic regime, the effect of the quadrupole coupling on the degree of alignment is very weak in the presence of the field. After the laser field is switched off, the quadrupole-free alignment shows a typical revival structure. For the linear  $I_2$  molecules,  $\langle \cos^2\theta \rangle$  at the full revival  $t = \tau_{\text{rot}}$

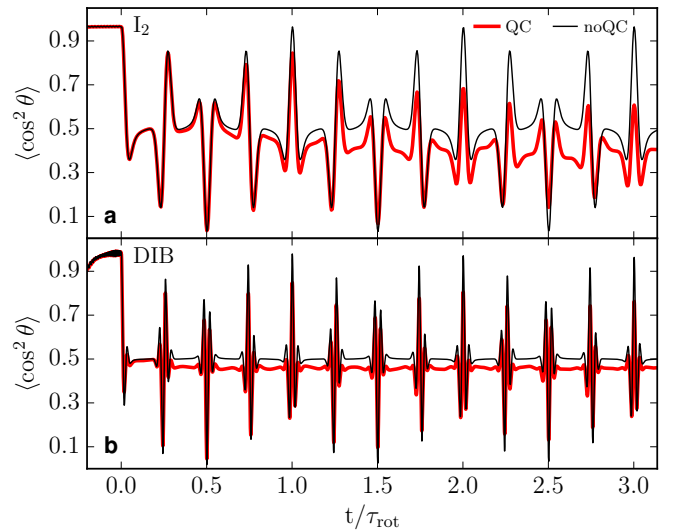


FIG. 2. Truncated pulse alignment with and without quadrupole coupling (QC and noQC) as a function of  $t/\tau_{\text{rot}}$  for (a)  $I_2$  and (b) DIB following a truncated laser pulse with a maximum laser intensity of  $I_0 = 5 \times 10^{11} \text{ W/cm}^2$ . The rising and falling edges of the pulse had Gaussian shapes with  $\tau_{\text{FWHM}} = 600$  ps and 2 ps, respectively.

reaches the same value as during the pulse,  $\langle \cos^2\theta \rangle = 0.96$ . Analogous behavior was observed for DIB with  $\langle \cos^2\theta \rangle = 0.98$ . Note that such high degrees of the post-pulse alignment for DIB are generally possible because the molecule is a near symmetric-top with only small populations of states with  $K_a > 0$ , effectively reducing the dynamics to that of a linear rotor. Generally, the peak alignment of asymmetric top molecules at the full revival does not reach the same value as at the peak intensity of the truncated pulse.<sup>27,29</sup>

For both molecules, the dephasing due to the nuclear-quadrupole coupling is comparable to the impulsive alignment case with intermediate intensities, see Fig. 1 b, f. For DIB, the inter- $J$  coupling due to quadrupole interaction noticeably influences the populations of rotational states during the pulse, where the dynamics shows nonadiabatic behavior. The alignment then starts to slightly deviate from the quadrupole-free results directly after the truncation of the laser field. By including the coupling, the strongest peak alignment was observed at the full revival  $t = \tau_{\text{rot}}$  with  $\langle \cos^2\theta \rangle = 0.85$  (0.84) for  $I_2$  (DIB), which is larger than the peak alignment obtained in the impulsive regime, see Fig. 1 d, h. However, the enhancement of the post-pulse alignment by using truncated laser pulses instead of impulsive-kick pulses was much smaller than without the quadrupole interaction.

**Post-pulse dynamics of excited rotational states** While state-selected molecular beams<sup>20,24,51–55</sup> or ultracold-molecules techniques<sup>56,57</sup> can produce near-0 K samples, this is not generally feasible, especially not for the heavy organic molecules discussed here. There-

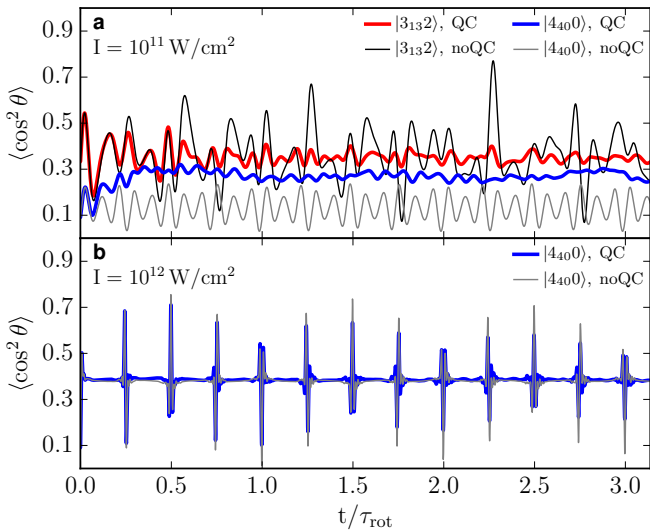


FIG. 3. Impulsive alignment for the initial states  $|3_{13}2\rangle$  and  $|4_{40}0\rangle$  of DIB including the quadrupole coupling (QC) and neglecting it (noQC) as a function of  $t/\tau_{\text{rot}}$ . The duration of the laser pulse is  $\tau_{\text{FWHM}} = 1$  ps and (a)  $I_0 = 1 \times 10^{11} \text{ W/cm}^2$  and (b)  $I_0 = 1 \times 10^{12} \text{ W/cm}^2$ .

fore, we investigated the impulsive-alignment dynamics for several initially excited states of  $\text{I}_2$  and DIB. Since comparable results were obtained for both molecules, we focus our analysis on DIB, namely the rotational states  $|J_{K_a K_c}, M_J\rangle = |3_{13}, 2\rangle$  and  $|4_{40}, 0\rangle$ . For both excited states, we observe a qualitatively similar influence of the quadrupole coupling as for the rotational ground state. For  $I_0 = 1 \times 10^{11} \text{ W/cm}^2$ ,  $\langle \cos^2 \theta \rangle$  in Fig. 3 a approaches  $1/3$  on timescales similar to the one in Fig. 1 e. For the higher intensity  $I_0 = 1 \times 10^{12} \text{ W/cm}^2$ , we find a more significant decrease of the post-pulse alignment for the initial state with  $J = 4, M_J = 0$ , Fig. 3 b than for the rotational ground state, Fig. 1 h. This can be attributed to the populations of field-free eigenstates, which are shifted toward smaller values of  $J$  for  $|4_{40}, 0\rangle$ . However, for other excited states the impact of the quadrupole coupling for higher laser intensities can be smaller, as is the case for  $|3_{13}2\rangle$ . Thus, for a thermal ensemble of molecules, we expect a small influence of nuclear-quadrupole interactions on the post-pulse alignment induced by strong laser fields. However, to accurately describe the alignment the coupling cannot be fully neglected even in this regime. Furthermore, on longer timescales even small frequency shifts will lead to a significant decrease of the alignment.<sup>30</sup>

#### IV. Summary and Conclusions

In conclusion, a significant dephasing of rotational wave packets was observed in the post-pulse dynamics for different laser-field shapes and intensities. The influence on the degree of alignment is the largest if low-energy, small- $J$  rotational states dominate the dynamics and diminishes

for highly excited states. For initially excited rotational states, the quadrupole coupling has a similar effect on the post-pulse dynamics as for the rotational ground state, which we expect to hold for thermal ensembles as well. Adiabatic alignment is essentially not affected by the nuclear-quadrupole interactions.

Our results emphasize the need to take into account the nuclear-quadrupole interactions in the description of field-free alignment for molecules with heavy nuclei with large nuclear quadrupoles. Since many biomolecules include such heavy elements, we plan to investigate other molecular species and their properties including rotational constants and molecular symmetry in the context of nuclear-quadrupole interactions.

## Appendix

### A. Spin-statistical weights of hyperfine states

To derive the weights of the iodine-spin-rotational wave functions of DIB, we made use of its molecular symmetry group  $D_{2h}$ , the corresponding character table can be found elsewhere.<sup>58</sup> Pure rotational states obey either  $A_g$ ,  $B_{1g}$ ,  $B_{2g}$  or  $B_{3g}$  symmetry, while the iodine nuclear-spin functions  $|I\rangle$  obey  $A_g$  or  $B_{1u}$  symmetry for  $I$  odd or even, respectively. This follows from the effect of symmetry operations  $\hat{P}$  that involve a permutation of the iodine nuclei,  $\hat{P}|I\rangle = (-1)^{I_1+I_2+I}|I\rangle$ , yielding a sign change for even values of  $I$ . The representation generated by the hydrogen nuclear-spin functions was derived<sup>58</sup> as  $7A_g \oplus 3B_{1g} \oplus 3B_{2g} \oplus 3B_{3g}$ . We considered rotational states having either  $A_g$  ( $|J_{K_a K_c}\rangle = |0_{00}\rangle$  and  $|4_{40}\rangle$ ) or  $B_{2g}$  ( $|3_{13}\rangle$ ) symmetry. With the requirement that the total internal wave function has to be of  $B_{1g}$  or  $B_{1u}$  symmetry, we obtained weights of 7 (3) for even (odd)  $I$  for the former case, while for the latter all spin-rotational states have equal weights.

In the case of the diatomic  $\text{I}_2$  molecule, there are no additional nuclear spins leading to degeneracies of the hyperfine levels. However, in the electronic and vibrational ground state considered here, states with  $J$  and  $I$  having opposite parities are forbidden due to the generalized symmetrization postulate.<sup>45</sup>

### Acknowledgments

We thank Andrey Duchko for his contributions in an early part of the project.

This work has been supported by the Deutsche Forschungsgemeinschaft (DFG) through the priority program ‘‘Quantum Dynamics in Tailored Intense Fields’’ (QUTIF, SPP1840, KU 1527/3, YA 610/1) and through the clusters of excellence ‘‘Center for Ultrafast Imaging’’ (CUI, EXC 1074, ID 194651731) and ‘‘Advanced Imaging of Matter’’ (AIM, EXC 2056, ID 390715994). R.G.F. gratefully acknowledges financial support by the

Spanish Project No. FIS2017-89349-P (MINECO), the Andalusian research group FQM-207, the Consejería de Conocimiento, Investigación y Universidad, Junta de Andalucía, and the European Regional Development Fund (ERDF, SOMM17/6105/UGR).

## References

- <sup>1</sup>Hamilton, E.; Seideman, T.; Ejdrup, T.; Poulsen, M. D.; Bisgaard, C. Z.; Viftrup, S. S.; Stapelfeldt, H. Alignment of symmetric top molecules by short laser pulses. *Phys. Rev. A* **2005**, *72*, 043402.
- <sup>2</sup>Rouzee, A.; Guerin, S.; Boudon, V.; Lavorel, B.; Faucher, O. Field-free one-dimensional alignment of ethylene molecule. *Phys. Rev. A* **2006**, *73*, 033418–9.
- <sup>3</sup>Rouzee, A.; Guerin, S.; Faucher, O.; Lavorel, B. Field-free molecular alignment of asymmetric top molecules using elliptically polarized laser pulses. *Phys. Rev. A* **2008**, *77*, 043412.
- <sup>4</sup>Trippel, S.; Mullins, T.; Müller, N. L. M.; Kienitz, J. S.; Omiste, J. J.; Stapelfeldt, H.; González-Férez, R.; Küpper, J. Strongly driven quantum pendulum of the carbonyl sulfide molecule. *Phys. Rev. A* **2014**, *89*, 051401(R).
- <sup>5</sup>Trippel, S.; Mullins, T.; Müller, N. L. M.; Kienitz, J. S.; González-Férez, R.; Küpper, J. Two-state wave packet for strong field-free molecular orientation. *Phys. Rev. Lett.* **2015**, *114*, 103003.
- <sup>6</sup>Thesing, L. V.; Yachmenev, A.; González-Férez, R.; Küpper, J. Laser-induced alignment of weakly bound molecular aggregates. *Phys. Rev. A* **2018**, *98*, 053412.
- <sup>7</sup>Altkorn, R.; Zare, R. N.; Greene, C. H. Depolarization of optically prepared molecules by two randomly oriented spins. *Mol. Phys.* **1985**, *55*, 1–9.
- <sup>8</sup>Yan, C.; Kummel, A. C. Effect of hyperfine depolarization upon creation and detection of alignment in free-jet expansions via selective photodissociation. *J. Chem. Phys.* **1993**, *98*, 6869–6882.
- <sup>9</sup>Cool, T. A.; Hemmi, N. Hyperfine polarization quantum beats in cyanogen. *J. Chem. Phys.* **1995**, *103*, 3357–3366.
- <sup>10</sup>Zhang, J.; Riehn, C. W.; Dulligan, M.; Wittig, C. An experimental study of HF photodissociation: Spin-orbit branching ratio and infrared alignment. *J. Chem. Phys.* **1996**, *104*, 7027–7035.
- <sup>11</sup>Wouters, E. R.; Siebbeles, L. D.; Reid, K. L.; Buijsse, B.; van der Zande, W. J. Observation of fine structure and hyperfine structure depolarization in the photofragment anisotropy in triplet H<sub>2</sub>. *Chem. Phys.* **1997**, *218*, 309–323.
- <sup>12</sup>Sofikitis, D.; Rubio-Lago, L.; Martin, M. R.; Ankeny Brown, D. J.; Bartlett, N. C.-M.; Alexander, A. J.; Zare, R. N.; Rakitzis, T. P. Optical control of ground-state atomic orbital alignment: Cl(<sup>2</sup>P<sub>3/2</sub>) atoms from HCl( $\nu = 2, J = 1$ ) photodissociation. *J. Chem. Phys.* **2007**, *127*, 144307.
- <sup>13</sup>Bartlett, N. C.-M.; Miller, D. J.; Zare, R. N.; Alexander, A. J.; Sofikitis, D.; Rakitzis, T. P. Time-dependent depolarization of aligned HD molecules. *Phys. Chem. Chem. Phys.* **2009**, *11*, 142–147.
- <sup>14</sup>Bartlett, N. C.-M.; Jankunas, J.; Zare, R. N.; Harrison, J. A. Time-dependent depolarization of aligned D<sub>2</sub> caused by hyperfine coupling. *Phys. Chem. Chem. Phys.* **2010**, *12*, 15689–15694.
- <sup>15</sup>Grygoryeva, K.; Rakovský, J.; Votava, O.; Fárnik, M. Imaging of rotational wave-function in photodissociation of rovibrationally excited HCl molecules. *J. Chem. Phys.* **2017**, *147*, 013901.
- <sup>16</sup>Loesch, H. J.; Remscheid, A. Brute force in molecular reaction dynamics: A novel technique for measuring steric effects. *J. Chem. Phys.* **1990**, *93*, 4779.
- <sup>17</sup>Friedrich, B.; Herschbach, D. Enhanced orientation of polar molecules by combined electrostatic and nonresonant induced dipole forces. *J. Chem. Phys.* **1999**, *111*, 6157.
- <sup>18</sup>Stapelfeldt, H.; Seideman, T. Colloquium: Aligning molecules with strong laser pulses. *Rev. Mod. Phys.* **2003**, *75*, 543–557.
- <sup>19</sup>Spence, J. C. H.; Doak, R. B. Single molecule diffraction. *Phys. Rev. Lett.* **2004**, *92*, 198102.
- <sup>20</sup>Filsinger, F.; Meijer, G.; Stapelfeldt, H.; Chapman, H.; Küpper, J. State- and conformer-selected beams of aligned and oriented molecules for ultrafast diffraction studies. *Phys. Chem. Chem. Phys.* **2011**, *13*, 2076–2087.
- <sup>21</sup>Reid, K. L. Accessing the molecular frame through strong-field alignment of distributions of gas phase molecules. *Phil. Trans. R. Soc. A* **2018**, *376*, 20170158–10.
- <sup>22</sup>Seideman, T. Revival structure of aligned rotational wave packets. *Phys. Rev. Lett.* **1999**, *83*, 4971–4974.
- <sup>23</sup>Rosca-Pruna, F.; Vrakking, M. J. J. Revival structures in picosecond laser-induced alignment of I<sub>2</sub> molecules. II. Numerical modeling. *J. Chem. Phys.* **2002**, *116*, 6579.
- <sup>24</sup>Karamatskos, E. T.; Raabe, S.; Mullins, T.; Trabattoni, A.; Stammer, P.; Goldsztejn, G.; Johansen, R. R.; Długołęcki, K.; Stapelfeldt, H.; Vrakking, M. J. J.; Trippel, S.; Rouzée, A.; Küpper, J. Molecular movie of ultrafast coherent rotational dynamics of OCS. *Nat. Commun.* **2019**, *10*, 3364.
- <sup>25</sup>T. Seideman, On the dynamics of rotationally broad, spatially aligned wave packets. *J. Chem. Phys.* **2001**, *115*, 5965.
- <sup>26</sup>Underwood, J.; Spanner, M.; Ivanov, M.; Mottershead, J.; Sussman, B.; Stolow, A. Switched wave packets: A route to nonperturbative quantum control. *Phys. Rev. Lett.* **2003**, *90*, 223001.
- <sup>27</sup>Underwood, J.; Sussman, B.; Stolow, A. Field-free three dimensional molecular axis alignment. *Phys. Rev. Lett.* **2005**, *94*, 143002.
- <sup>28</sup>Goban, A.; Minemoto, S.; Sakai, H. Laser-field-free molecular orientation. *Phys. Rev. Lett.* **2008**, *101*, 013001.
- <sup>29</sup>Chatterley, A.; Karamatskos, E. T.; Schouder, C.; Christiansen, L.; Jörgensen, A. V.; Mullins, T.; Küpper, J.; Stapelfeldt, H. Switched wave packets with spectrally truncated chirped pulses. *J. Chem. Phys.* **2018**, *148*, 221105.
- <sup>30</sup>Thomas, E. F.; Søndergaard, A. A.; Shepperson, B.; Henriksen, N. E.; Stapelfeldt, H. Hyperfine-Structure-Induced Depolarization of Impulsively Aligned I<sub>2</sub> Molecules. *Phys. Rev. Lett.* **2018**, *120*, 163202.
- <sup>31</sup>Yachmenev, A.; Thesing, L. V.; Küpper, J. Laser-induced dynamics of molecules with strong nuclear quadrupole coupling. *J. Chem. Phys.* **2019**, *151*, 244118.
- <sup>32</sup>Weigend, F.; Furche, F.; Ahlrichs, R. Gaussian basis sets of quadruple zeta valence quality for atoms H–Kr. *J. Chem. Phys.* **2003**, *119*, 12753–12762.
- <sup>33</sup>Weigend, F.; Ahlrichs, R. Balanced basis sets of split valence, triple zeta valence and quadruple zeta valence quality for H to Rn: Design and assessment of accuracy. *Phys. Chem. Chem. Phys.* **2005**, *7*, 3297.
- <sup>34</sup>Peterson, K. A.; Figgen, D.; Goll, E.; Stoll, H.; Dolg, M. Systematically convergent basis sets with relativistic pseudopotentials. II. Small-core pseudopotentials and correlation consistent basis sets for the post-d group 16–18 elements. *J. Chem. Phys.* **2003**, *119*, 11113–11123.
- <sup>35</sup>Neese, F. The ORCA program system. *Wiley Interdiscip. Rev. Comput. Mol. Sci.* **2011**, *2*, 73–78.
- <sup>36</sup>Neese, F. Software update: the ORCA program system, version 4.0. *Wiley Interdiscip. Rev. Comput. Mol. Sci.* **2017**, *8*, e1327.
- <sup>37</sup>Pyykkö, P. Year-2008 nuclear quadrupole moments. *Mol. Phys.* **2008**, *106*, 1965–1974.
- <sup>38</sup>Yokozeki, A.; Muentner, J. S. Laser fluorescence state selected and detected molecular beam magnetic resonance in I<sub>2</sub>. *J. Chem. Phys.* **1980**, *72*, 3796–3804.
- <sup>39</sup>Owens, A.; Yachmenev, A. RichMol: A general variational approach for rovibrational molecular dynamics in external electric fields. *J. Chem. Phys.* **2018**, *148*, 124102.
- <sup>40</sup>Maroulis, G.; Makris, C.; Hohm, U.; Goebel, D. Electrooptical Properties and Molecular Polarization of Iodine, I<sub>2</sub>. *J. Phys. Chem. A* **1997**, *101*, 953–956.
- <sup>41</sup>For convenience and tradition, we specify polarizabilities in Å<sup>3</sup>, which can easily be converted to SI units as 1Å<sup>3</sup> = 10<sup>6</sup> pm<sup>3</sup>.
- <sup>42</sup>Neese, F.; Wolf, A.; Fleig, T.; Reiher, M.; Hess, B. A. Calculation of electric-field gradients based on higher-order generalized Douglas–Kroll transformations. *J. Chem. Phys.* **2005**, *122*, 204107.
- <sup>43</sup>Jorge, F. E.; Neto, A. C.; Camiletti, G. G.; Machado, S. F. Contracted Gaussian basis sets for Douglas–Kroll–Hess calculations:

- Estimating scalar relativistic effects of some atomic and molecular properties. *J. Chem. Phys.* **2009**, *130*, 064108.
- <sup>44</sup>Campos, C.; Jorge, F. Triple zeta quality basis sets for atoms Rb through Xe: application in CCSD(T) atomic and molecular property calculations. *Mol. Phys.* **2012**, *111*, 167–173.
- <sup>45</sup>Kroll, M. Hyperfine Structure in the Visible Molecular-Iodine Absorption Spectrum. *Phys. Rev. Lett.* **1969**, *23*, 631–633.
- <sup>46</sup>Cook, R. L.; de Lucia, F. C. Application of the Theory of Irreducible Tensor Operators to Molecular Hyperfine Structure. *Am. J. Phys.* **1971**, *39*, 1433–1454.
- <sup>47</sup>Yachmenev, A.; Küpper, J. Communication: General variational approach to nuclear-quadrupole coupling in rovibrational spectra of polyatomic molecules. *J. Chem. Phys.* **2017**, *147*, 141101.
- <sup>48</sup>Holmegaard, L.; Viftrup, S. S.; Kumarappan, V.; Bisgaard, C. Z.; Stapelfeldt, H.; Hamilton, E.; Seideman, T. Control of rotational wave-packet dynamics in asymmetric top molecules. *Phys. Rev. A* **2007**, *75*, 051403.
- <sup>49</sup>Gordy, W.; Cook, R. L. *Microwave Molecular Spectra*, 3rd ed.; John Wiley & Sons: New York, NY, USA, 1984.
- <sup>50</sup>Kroto, H. W. *Molecular Rotation Spectra*; Dover Publications, Inc.: Mineola, NY, USA, 2003.
- <sup>51</sup>Hutzler, N. R.; Lu, H.-I.; Doyle, J. M. The buffer gas beam: An intense, cold, and slow source for atoms and molecules. *Chem. Rev.* **2012**, *112*, 4803–4827.
- <sup>52</sup>van de Meerakker, S. Y. T.; Bethlem, H. L.; Vanhaecke, N.; Meijer, G. Manipulation and Control of Molecular Beams. *Chem. Rev.* **2012**, *112*, 4828–4878.
- <sup>53</sup>Chang, Y.-P.; Horke, D. A.; Trippel, S.; Küpper, J. Spatially-controlled complex molecules and their applications. *Int. Rev. Phys. Chem.* **2015**, *34*, 557–590.
- <sup>54</sup>Nielsen, J. H.; Simesen, P.; Bisgaard, C. Z.; Stapelfeldt, H.; Filsinger, F.; Friedrich, B.; Meijer, G.; Küpper, J. Stark-selected beam of ground-state OCS molecules characterized by revivals of impulsive alignment. *Phys. Chem. Chem. Phys.* **2011**, *13*, 18971–18975.
- <sup>55</sup>Horke, D. A.; Chang, Y.-P.; Długołęcki, K.; Küpper, J. Separating Para and Ortho Water. *Angew. Chem. Int. Ed.* **2014**, *53*, 11965–11968.
- <sup>56</sup>Ulmanis, J.; Deiglmayr, J.; Repp, M.; Wester, R.; Weidemüller, M. Ultracold Molecules Formed by Photoassociation: Heteronuclear Dimers, Inelastic Collisions, and Interactions with Ultrashort Laser Pulses. *Chem. Rev.* **2012**, *112*, 4890–4927.
- <sup>57</sup>Quéméner, G.; Julienne, P. S. Ultracold Molecules under Control! *Chem. Rev.* **2012**, *112*, 4949–5011.
- <sup>58</sup>Bunker, P. R.; Jensen, P. *Molecular Symmetry and Spectroscopy*, 2nd ed.; NRC Research Press: Ottawa, Ontario, Canada, 1998.